



HAL
open science

Iron and Copper Containing Oxygen Reduction Catalysts from Templated Glucose-Histidine.

Ivano Galbiati, Claudia Letizia Bianchi, Mariangela Longhi, Leonardo Formaro

► **To cite this version:**

Ivano Galbiati, Claudia Letizia Bianchi, Mariangela Longhi, Leonardo Formaro. Iron and Copper Containing Oxygen Reduction Catalysts from Templated Glucose-Histidine.. Fuel Cells, 2010, 10 (2), pp.251. 10.1002/fuce.200900142 . hal-00552363

HAL Id: hal-00552363

<https://hal.science/hal-00552363>

Submitted on 6 Jan 2011

HAL is a multi-disciplinary open access archive for the deposit and dissemination of scientific research documents, whether they are published or not. The documents may come from teaching and research institutions in France or abroad, or from public or private research centers.

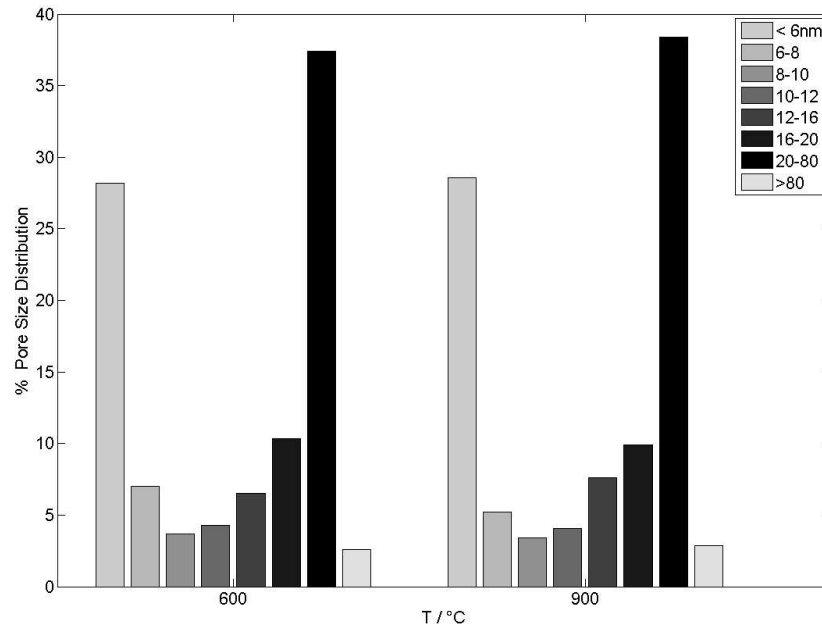
L'archive ouverte pluridisciplinaire **HAL**, est destinée au dépôt et à la diffusion de documents scientifiques de niveau recherche, publiés ou non, émanant des établissements d'enseignement et de recherche français ou étrangers, des laboratoires publics ou privés.



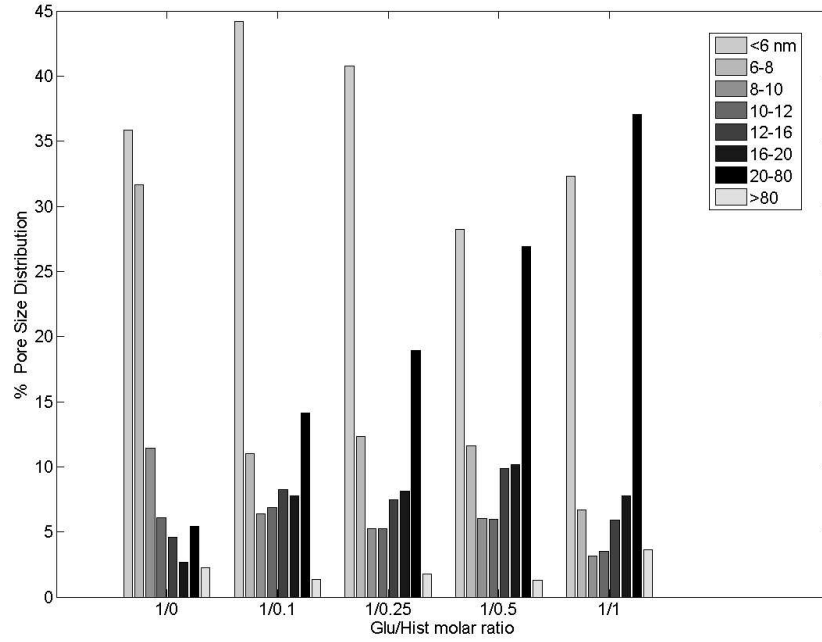
Iron and Copper Containing Oxygen Reduction Catalysts from Templated Glucose-Histidine.

Journal:	<i>Fuel Cells</i>
Manuscript ID:	face.200900142.R1
Wiley - Manuscript type:	Original Research Paper
Date Submitted by the Author:	27-Oct-2009
Complete List of Authors:	Galbiati, Ivano Bianchi, Claudia Longhi, Mariangela; Università degli Studi di Milano, Chimica Fisica ed Electrochimica Formaro, Leonardo
Keywords:	Oxygen Reduction Reaction, Platinum-free Catalysts, C/N/Me centers, Iron-Copper, Hard Templating





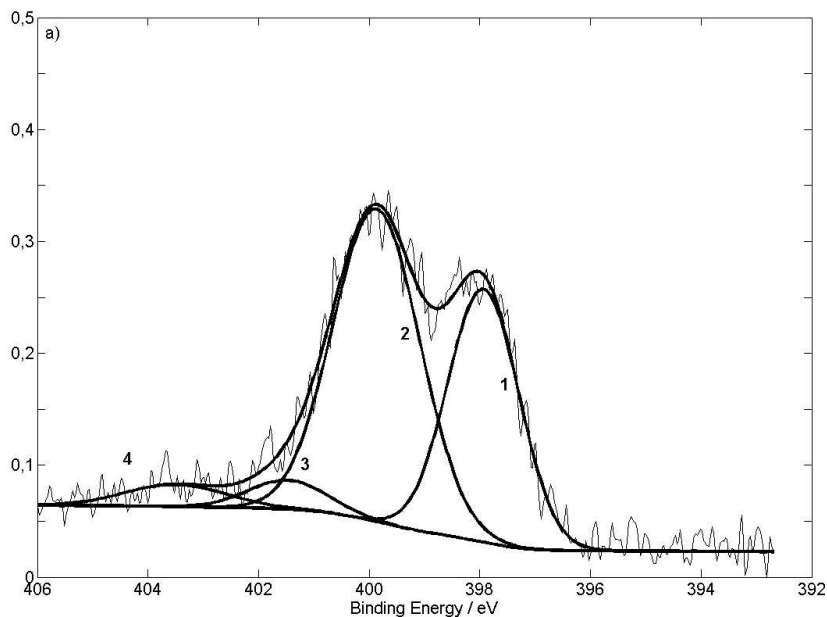
Pore Size Distributions at different temperatures. GluHistFe75.
338x238mm (96 x 96 DPI)



Pore Size Distributions at various Glu/Hist molar ratios (T= 600°C).
338x243mm (96 x 96 DPI)

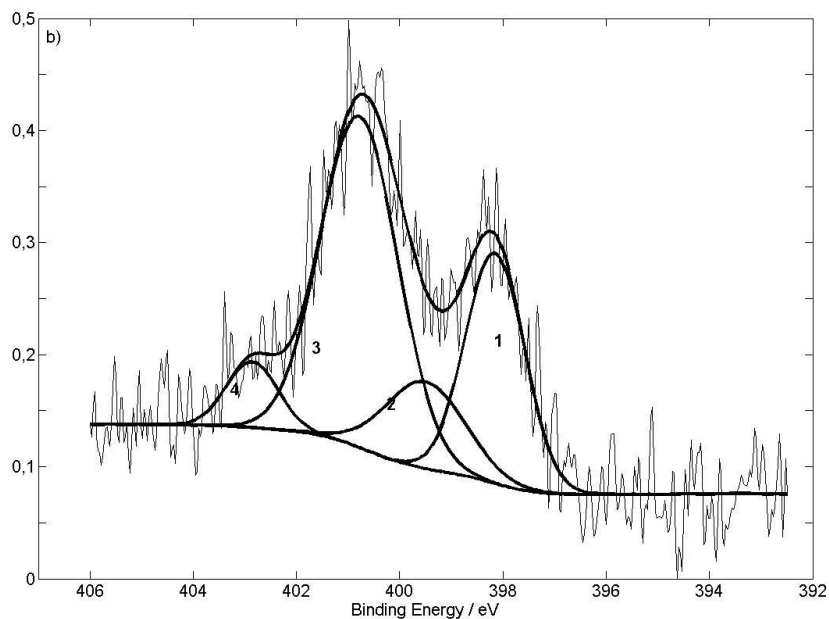
Review

1
2
3
4
5
6
7
8
9
10
11
12
13
14
15
16
17
18
19
20
21
22
23
24
25
26
27
28
29
30
31
32
33
34
35
36
37
38
39
40
41
42
43
44
45
46
47
48
49
50
51
52
53
54
55
56
57
58
59
60



High resolution Nitrogen (1s) Spectra of GluHist: a) T= 600°C; 1) pyridinic N (N6) (B.E. 398 -398.4 eV); 2) pyrrolic-N in five member ring and or pyridonic-N (N5) (B.E. 400-400.5 eV); 3) quaternary-N (NQ), e.g. N in graphene structure (B.E. 401.5-402.2 eV); 4) pyridinic-N-oxide (NX) (B.E. 403.5-404.8 eV) B.E. are from [45-48].

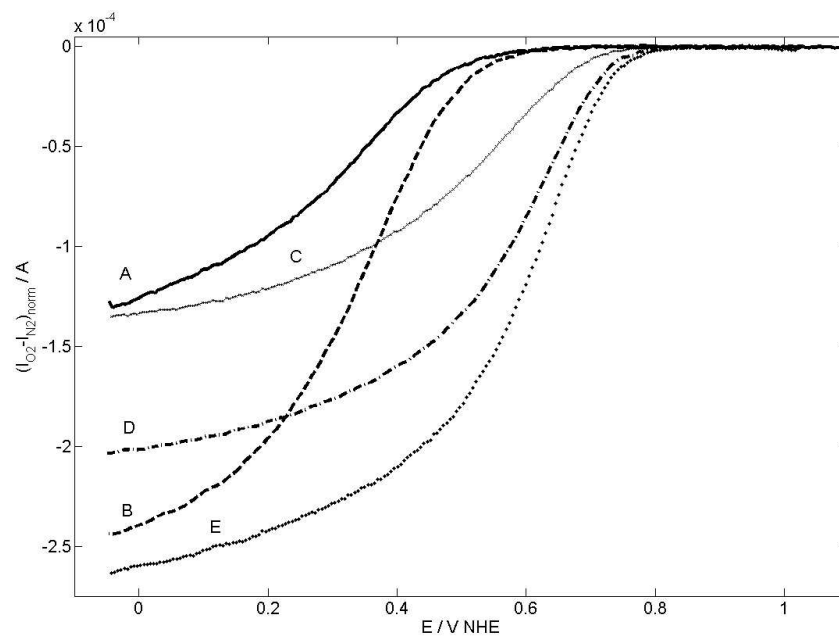
338x232mm (96 x 96 DPI)



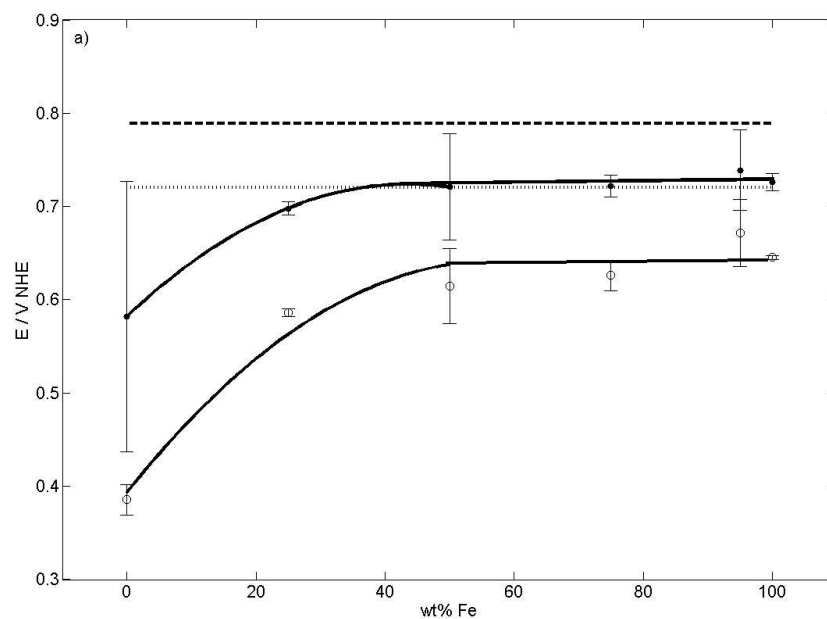
31 High resolution Nitrogen (1s) Spectra of GluHist: b) T= 900°C. 1) pyridinic N (N6) (B.E. 398 -398.4
32 eV); 2) pyrrolic-N in five member ring and or pyridonic-N (N5) (B.E. 400-400.5 eV); 3) quaternary-
33 N (NQ), e.g. N in graphene structure (B.E. 401.5-402.2 eV); 4) pyridinic-N-oxide (NX) (B.E. 403.5-
34 404.8 eV) B.E. are from [45-48].

35 338x232mm (96 x 96 DPI)

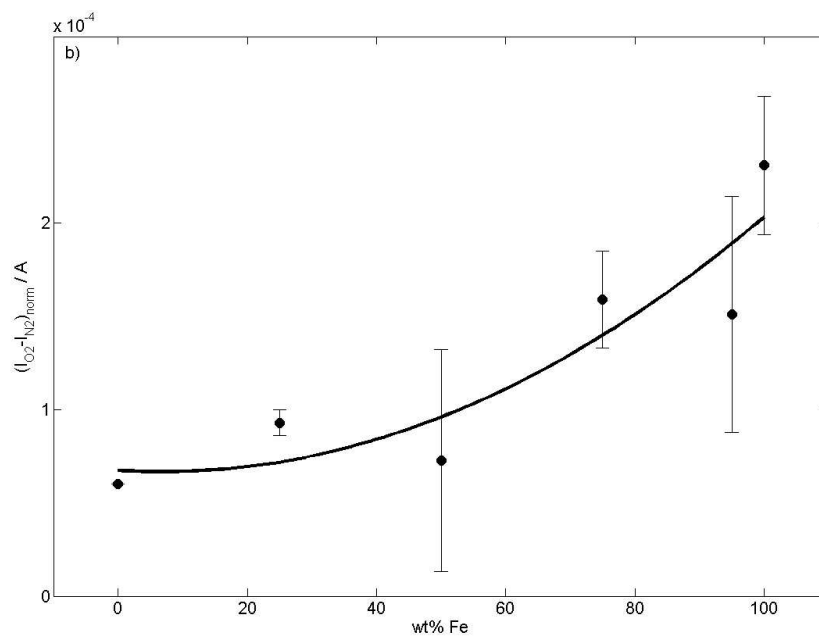
36
37
38
39
40
41
42
43
44
45
46
47
48
49
50
51
52
53
54
55
56
57
58
59
60



Voltammograms in oxygen-saturated 0.1M HClO₄. A) GluHist; B) GluHistFe0; C) GluHistFe25; D) GluHist75; E) GluHistFe100. (T=25°C; scan rate 5 mV s⁻¹; rotation rate 700 rpm).
338x232mm (96 x 96 DPI)



a) Incipient oxygen reduction potentials at different Fe wt %: ● and --- (heavy dashes) potentials at the intersection points in Fig. 5; ○ and --- (light dashes) peak potentials of cathodic maxima at $\omega=0$ rpm. Dashes are for EC-20 Pt catalyst, open and closed points are for home made carbons.
338x232mm (96 x 96 DPI)



31 b) Currents at $E=+0.420$ V NHE at different wt % Fe.
32 Lines are a guide to the eye. Error bars represent standard deviation of experimental data. (0.1M
33 HClO₄, scan rate 5 mV s⁻¹, rotation rate 700 rpm, T= 25°C.)
34

35 338x232mm (96 x 96 DPI)

1
2
3
4
5
6
7 **Iron and Copper Containing Oxygen Reduction Catalysts**
8 **from Templated Glucose-Histidine.**
9

10
11
12 Ivano Galbiati, Claudia L. Bianchi, Mariangela Longhi*, **Andrea Carrà**, Leonardo
13 Formaro
14

15
16
17 Dipartimento di Chimica Fisica ed Elettrochimica, Università degli Studi di Milano, Via
18 Golgi 19, 20133 Milano Italy
19

20
21
22
23
24
25
26
27
28
29
30
31
32
33
34
35
36
37
38
39
40
41 *[*] Corresponding author, Email: mariangela.longhi@unimi.it*
42
43
44
45
46
47
48
49
50
51
52
53
54
55
56
57
58
59
60

Abstract

Nitrogen doped carbons loaded with non-precious transition metals are currently investigated as substitutes of Pt-based catalysts for oxygen reduction in Polymer Electrolyte Fuel Cells (PEMFC's). This paper reports the preparation of one kind of such catalysts using glucose/histidine mixtures added with Fe and Cu salts in the presence of silica gels as hard templating agent to increase carbon surface area. The resulting carbons contain nitrogen in amounts that depend on heating temperature ($T=600$ and $T=900^{\circ}\text{C}$) on the glucose/histidine molar ratio and, more weakly, on the relative Fe/Cu amount. Surface areas are a function of reactant concentration and heating temperature, whereas pore size and pore size distribution only depend on glucose-histidine molar ratio. Cyclic voltammetry results on oxygen reduction depend on Fe/Cu ratio, the best result both in terms of incipient oxygen reduction potentials and currents being observed on samples only containing Fe, with no Cu added.

Keywords: Oxygen Reduction Reaction, Platinum-free Catalysts, C/N/Me centers, Iron-Copper, Hard Templating,

1. Introduction

Fuel cells, and more specifically PEMFC's, represent promising power systems to the world economy, with many applications and low environmental impact. A most important aspect concerning their widespread implementation is the cost of both polymeric membranes and catalytic electrode materials which are necessary to promote electrode reactions thus increasing fuel cell energy efficiency. This is especially true for the cathodic oxygen reaction (ORR), the best catalyst being at present based on the very expensive platinum metal or Pt-alloys (about 2250 \$/oz [1]). Therefore, a decrease in Pt amount (from 1.1 to 0.2 g/KW in 2015, DOE data [2]) or its replacement with non-precious materials having comparable performance is necessary. Research on this subject started in the '60s [3] with a notable turning point from Yeager's work at the end of '80s [4], and became a worldwide continuing issue with contributions from many authoritative research groups.

Among various materials, nitrogen modified carbons also containing non-precious transition metals (Fe and Co) are considered interesting because of their ORR activity and reliability as confirmed by results from independent groups [5-15]. Several preparative methods are reported: 1) carbon impregnation with metal organosalts or cyanoderivatives, followed by thermal activation in the presence of e.g. ammonia gas [5]; 2) thermal treatment of nitrogen-containing metal complexes adsorbed onto carbon [16-36]; 3) polymerization of aromatic compounds, e.g. pyrrole [37,38], onto carbon surface followed by metal ion adsorption (Co^{2+}) to obtain porphyrine-like structures; 4) thermal treatment of mixed precursors from a carbon and nitrogen source, respectively, e.g. glucose and an amino acid, added with transition metal salts (Fe,Cu) [9,14]. These latter materials are considered interesting because of the ease and flexibility of the

1
2
3
4
5
6 synthetic route and, moreover, of the catalytic activity, with incipient oxygen reduction
7
8 potentials closely approaching (by ~40 mV) those of commercial Pt catalysts [14].
9

10 Unfortunately, however, they are reported with low stability [14].

11
12 Recently, thermodynamic criteria were put forward to model the catalytic activity of Pt-
13 free bimetallic alloys [39] permitting to evaluate what metal, or combination of metals,
14
15 may be most effective in ORR. As a result $\text{Fe}^{2+}/\text{Cu}^{+}$ ions were shown most favourable.
16
17 Interestingly these ions are also present in natural enzymatic systems like cytochrome C
18
19 oxidase, an effective and selective catalyst in the reduction of oxygen to H_2O , based on
20
21 a cooperative effect of the two ions.
22
23
24
25

26
27 Improving catalyst activity is not only a matter of varying composition but also involves
28 morphological/textural aspects. By reference to carbon supported Pt catalysts, carbon
29 origin, surface area, porosity and pore size distribution reportedly affect end material
30 performances. Reviewing these aspects, Antolini [40] has recently shown that besides
31 good electrical conductivity, carbon supports have to be characterized by high surface
32 areas and high fractional pore percentage in the mesoporosity region (2-50 nm) in order
33
34 to favour reactant mass transport to and from catalytic centers, the more so if the
35
36 catalytic sites are preferentially located at inner positions of the carbon structure, in the
37
38 micropore size region as reported by [41].
39
40
41
42
43
44
45
46
47

48 Histidine was chosen as the nitrogen-bearing precursor, because it contains both an
49
50 imidazolic ring and a carboxyl group that, if retained in end products upon thermal
51
52 activation, may presumably contribute to ORR activity [40-42]. In the attempt of
53
54 increasing carbon surface area and at the same time controlling porosity in the
55
56 mesoporosity range a hard template method was adopted using silica gel suspensions in
57
58
59
60

1
2
3
4
5
6 water. Also, Fe^{2+} and Cu^{2+} in variable ratios were used to explore the entire composition
7
8 range as suggested by the theoretical examination in [39].
9

10 11 12 2. Experimental

13 14 15 2.1. Reagents

16
17 Glucose, histidine, Fe(II) acetate, Cu(II) acetate, glacial acetic acid and Nafion (5 wt %
18
19 solution) were purchased from Aldrich and used as received. Silica (Silica Gel 60 HR)
20
21 and HClO_4 (60 wt %) were from Merck and Fluka, respectively. High purity water from
22
23 a MilliQ system (Millipore) was used throughout. Nitrogen and oxygen (Sapio, 5nines)
24
25 were used.
26
27

28 29 30 31 2.2. Preparation of the catalytic materials

32
33 A glucose (Glu in the following) solution in water (1.68 mol dm^{-3}) was added with
34
35 histidine (Hist) in variable molar ratios: Glu/Hist=1/1 is indicated as GluHist in the
36
37 following; Glu/Hist=2/1 as GluHist0.5; Glu/Hist=4/1 as GluHist0.25; Glu/Hist=10/1 as
38
39 GluHist0.1. Adding equimolar glacial acetic was found necessary to dissolve histidine.
40
41 10 ml of this solution were stirred with 4.3 g of silica for 5 min to form a gel, and stirred
42
43 again 5 min after 15 min standing. The gel was loaded in a quartz reactor, degassed with
44
45 N_2 ($100 \text{ cm}^3 \text{ min}^{-1}$) for about 5 min and inserted in a preheated vertical oven at
46
47 $T=600^\circ\text{C}$ in order to carbonize as fast as possible the precursors, preserving the ordered
48
49 room temperature gel structure in the final products. Heating was continued for 1 h
50
51 under continuous N_2 purging ($100 \text{ cm}^3 \text{ min}^{-1}$). Then the tube was rapidly quenched in
52
53 air. Silica was removed in 3M boiling NaOH followed by repeated carbon
54
55 washing/filtering (MilliQ water, $0.45 \mu\text{m}$ Durapore filters) until water conductivity
56
57
58
59
60

1
2
3
4
5
6 became lower than 4 μS . Products were dried in nitrogen (100 °C, 24 h) and finally
7
8 ground in an agate mortar. Metal containing catalysts were prepared by the same
9
10 procedure but for the addition of acetate metal salts (Fe and Cu ions at 1 wt % total with
11
12 respect to glucose+histidine, at variable ratios between them). The ratio of iron and
13
14 copper salts was varied in a range from 0% to 100% iron: GluHistFe0: 0% Fe/100 %
15
16 Cu; GluHistFe25: 25% Fe/75 % Cu; GluHistFe50: 50% Fe/50 % Cu; GluHistFe75: 75%
17
18 Fe/25 % Cu; GluHistFe95: 95% Fe/5 % Cu; GluHistFe100: 100% Fe/0 % Cu.
19
20
21

22 All materials were heat-activated in a second step at $T=900^\circ\text{C}$ under constant N_2 flow
23
24 ($100\text{ cm}^3\text{ min}^{-1}$) in the following conditions: 30 min room temperature purging, ramping
25
26 at 6°C min^{-1} and 3 h standing at $T=900^\circ\text{C}$, fast quenching to room temperature.
27
28
29
30
31

32 **2.3. Characterisation of materials**

33 *X-ray Photoelectron Spectroscopy (XPS).*

34 XPS measurements were performed with an M-Probe Instrument (SSI) equipped with a
35
36 monochromatic Al $\text{K}\alpha$ source (1486.6 eV) with a spot size of $200 \times 750\ \mu\text{m}$ and a pass
37
38 energy of 25 eV, providing a resolution of 0.74 eV. The energy scale was calibrated
39
40 with reference to the 4f_{7/2} level of a freshly evaporated gold sample ($84.00 \pm 0.1\text{ eV}$)
41
42 and to the 2p_{3/2} and 3s levels of copper (932.47 ± 0.1 and $122.39 \pm 0.15\text{ eV}$,
43
44 respectively). An electron flood gun was used to compensate for the buildup of positive
45
46 charge on insulating samples: a value of 5 eV was selected. For all samples, the C 1s
47
48 peak level was taken as the internal reference at 284.6 eV. Accuracy of reported binding
49
50 energies (BEs) is approximately $\pm 0.2\text{ eV}$. Quantitative data were carefully checked and
51
52 reproduced several times. Uncertainty in spectral decomposition is estimated to be $\pm 1\%$.
53
54
55
56
57
58
59
60

Specific Surface Area.

1
2
3
4
5
6 Surface area and porosity were determined by low temperature B.E.T. N₂ adsorption
7
8 using an SA3100 Coulter apparatus. Before measurement, samples were outgassed at
9
10 T= 80 °C for 3 h. Surface area and porosity were calculated from nitrogen isotherms
11
12 using the instrumental software (Version 2.12).
13
14

15
16
17 TEM images were obtained by a Zeiss EFTEM LEO 912AB (120 kV) microscope
18
19

20 21 22 **2.4. Electrode and catalyst layer preparation**

23
24 Electrochemical characterisation was performed by the Thin Film Rotating Disk
25
26 Electrode (TFRDE) method immobilizing small catalyst amounts onto the graphite tip
27
28 (geometric surface area: $A=0.0491 \text{ cm}^2$) of a rotating disk electrode (EDI 101,
29
30 Radiometer). Before use the tip was gently cleaned with soft sandpaper, polished by
31
32 diamond powder (Aldrich) and finally degreased with ethanol. Catalyst aliquots (8 mg)
33
34 were dispersed in water added with Nafion (1.5 ml water, 4 μl Nafion) and sonicated for
35
36 30 min; 7 μl of this mixture were pipetted onto the electrode tip and dried in a bottom-
37
38 up position above a tungsten lamp.
39
40
41
42

43 44 45 **2.5. Electrochemical measurements**

46
47 A two compartment cell with a graphite counterelectrode (Amel 201/S-016) and a
48
49 AgCl/Ag external reference electrode (Amel) in 3M NaCl was used. The reference was
50
51 connected to the cell by a salt bridge filled with the working electrolyte (0.1 M HClO₄).
52
53 Before each experimental run all glassware was washed by concentrated H₂SO₄ and
54
55 rinsed in MilliQ water. The counterelectrode was cleaned with filter paper. The
56
57 potentiostat was AMEL mod. 7050. **Measurements were performed by an accurately**
58
59 **reproducible procedure.** Before CV recording, the electrode was conditioned cycling 45
60

1
2
3
4
5
6 min in N₂ in the potential range E=-0.275 – +0.800 V, followed by 100 min cycling in
7
8 O₂ saturated solution (5 mV/s, ω =1600 rpm). Then O₂ reduction results were recorded
9
10 in the same conditions at different electrode rotation rates. To verify electrode stability
11
12 and internal reproducibility several CVs at ω = 1600 rpm were recorded in each run.
13
14 After measurements in O₂, CVs were again recorded in N₂ to obtain background
15
16 faradaic currents for O₂ reduction data correction. Background charge values were also
17
18 obtained by integration of N₂ curves and used as a measure of real electrode surface
19
20 area, normalizing the many investigated materials with respect to Glu (T=900°C) that
21
22 was assumed as an internal, arbitrary reference.
23
24
25
26
27

28 3. Results and Discussion.

29
30
31 In the presence of silica gel as a templating agent, carbon materials with expanded,
32
33 sponge-like overall morphology are obtained as shown in Fig. 1 for a plain glucose
34
35 sample heated at T=600 °C. These effects are more quantitatively observed in the first
36
37 two entry lines of Tab. 1 where the sample obtained in the presence of silica shows a
38
39 tremendous increase of BET surface area (1100 m²/g) instead of a few square meters/g
40
41 of the corresponding glucose-only sample. Though in the absence of comparison data
42
43 without added silica, Tab. 1 shows that similarly high BET areas are obtained for all the
44
45 samples. Interestingly, besides depending on silica, surface areas are a function of the
46
47 used reactant, reactant concentration and heating temperature. Most relevant effects are
48
49 due to histidine that, at even the lowest used molar ratio with respect to glucose (see
50
51 GluHist0.1 in Tab. 1), causes a surface area decrease of ~200 m²/g, with a further
52
53 decreasing trend taking place with increasing histidine/glucose molar ratio. Though
54
55 moderate, opposite effects arise from metal ion addition, with surface areas in any case
56
57 greater than the metal-free reference (sample GluHist) and also weakly increasing with
58
59
60

1
2
3
4
5
6 increasing the $\text{Fe}^{2+}/\text{Cu}^{2+}$ ratio. As expected on general grounds, and in accordance with
7
8 some matter loss visually observed as brownish gas emitted during the second heating at
9
10 $T=900\text{ }^\circ\text{C}$, surface areas decrease with increasing temperature. This decrease is in some
11
12 relation with surface areas from the previous heating at $T=600\text{ }^\circ\text{C}$. As a fact, the last
13
14 column in Tab. 1 shows that surface areas at $T=900$ and $T=600\text{ }^\circ\text{C}$ are in a ca. constant
15
16 ratio of 0.75-0.9. In a further aspect of this thermal behaviour, BET fractional pore
17
18 volume distributions of many samples were found essentially independent of heating
19
20 temperature. This is shown as an example in Fig. 2 for sample GluHistFe75. Then, the
21
22 above surface area ratio and the lack of variation in pore volume distribution appear
23
24 related, and jointly suggest that textural sample features are mostly established during
25
26 the first heating in the presence of silica, followed by lesser rearrangements taking place
27
28 at higher temperature after silica removal, these readjustments in their turn causing a
29
30 moderate decrease of previous surface areas while leaving essentially unchanged
31
32 porosity distribution.
33
34
35
36
37

38
39 Reactant composition effects on porosity are reported for the more extensively available
40
41 results at $T=600\text{ }^\circ\text{C}$. In Fig. 3 histidine addition causes readjustments of the pristine
42
43 glucose porosity, especially relevant at both the extremes of the accessible pore size
44
45 range. In the low size region, pores 6-8 nm in size undergo a first redistribution in
46
47 favour of the smaller ones (6 nm). Though with irregular variations, pores with these
48
49 latter size are a large fractional value regardless of increasing histidine amounts. At the
50
51 other extreme of size, increasing histidine causes the 20-80 nm pore size to become
52
53 gradually more abundant, up to ~35% of the overall sample porosity. Adding Fe^{2+} and
54
55 Cu^{2+} ions in variable relative amounts has no apparent effect (not reported) on the
56
57 porosity distribution of a number of carbons with constant Glu/Hist ratio
58
59
60

1
2
3
4
5
6 (Glu/Hist=1/1). Histidine is therefore most effective to promote pore size increase. This
7
8 is at variance with Maruyama's results [9] on similar glucose/adenine carbons from a
9
10 "dry" procedure without templates.
11

12
13
14
15 XPS survey results are shown in Tab. 2. Cu and Fe are undetected even for the lower
16
17 used heating temperature. This situation is frequently observed, and unresolved, in the
18
19 literature with the baffling outcome that, though undetected in outermost surface layers,
20
21 added metals are indeed effective in promoting electrochemical ORR carbon behaviour.
22
23 As also representative of the present results, we mention that Fe was undetected by both
24
25 XPS and UPS [43] in spite of wide variation in added amounts, the maximum Fe value
26
27 reaching 5.5 wt % with respect to the graphite oxide that was used in that case.
28
29

30
31
32 Moreover, in [44] it is reported that "after carbonization, the content of copper
33
34 decreases as the copper ions are reduced into metallic copper nanoparticles. These
35
36 nanoparticles are difficult to detect by XPS because they are coated by a thin carbon
37
38 layer and migrate into the carbon matrix". As observed in Tab. 2 for samples heated at
39
40 both T=600 and 900 °C, the relative abundance of C1s and N1s signals is moreover
41
42 only weakly affected by metal addition.
43
44

45
46 Tab. 2 shows that N1s signals of GluHist (T=600 °C) are initially very high (14%) and
47
48 decrease with both increasing temperature (7%, T=900 °C) and decreasing the histidine
49
50 amount adopted in preparation (4%, Glu/Hist0.10). Notably, the temperature-dependent
51
52 nitrogen decrease is accompanied by increasing C1s signals (from 82 to 91%) showing
53
54 that nitrogen removal also induces chemical carbon readjustments. Fig. 4 and Tab. 3
55
56 evidence that different nitrogen forms are present (Fig. 4a) with variable and
57
58 temperature-dependent relative amounts (Fig. 4b). In GluHist for T=600 °C two main
59
60

1
2
3
4
5
6 contributions are due to pyridinic (N6) and pyrrolic/pyridonic (N5) forms, in relative
7
8 amounts of 36 and 55 atomic %, respectively. Minor contributions are due to
9
10 quaternary-N (NQ, ~5%), and pyridinic-N-oxide (NX, 4%) (Relevant binding energies,
11
12 B.E., are reported in the caption to Fig. 4 [45-48]). All these nitrogen forms undergo
13
14 extensive redistribution upon heating to T=900 °C, with N6 that decreases by ~25%, N5
15
16 by ~75%, such variations being counteracted by an extraordinary, tenfold increase of
17
18 NQ, and doubling of NX. These readjustments are in accordance with literature data
19
20 [48] by which N5 and N6 are thermally unstable with respect to NQ. This latter NQ
21
22 represents a class of compounds in which substitutional nitrogen in graphene layers is
23
24 theoretically advocated [49, 50] as active for ORR on metal-free catalysts.
25
26
27
28

29
30 However, results in Tab. 3 show that adding metals (Fe, Cu) to glucose-histidine
31
32 precursors surprisingly does not cause a decrease in N5 and N6 signals with the
33
34 increasing heating temperature, which would be expected from all the above literature
35
36 data. This behaviour may be attributed to the formation of metal complexes from N5
37
38 and N6 groups, which indirectly corresponds to their thermal stabilization. In support of
39
40 this hypothesis, it can be mentioned that in a recent paper [51] the signal at 399.3 eV,
41
42 which is consistent with the present N5 and N6 species, was attributed to iron-
43
44 associated pyridinic nitrogen species. This evidence can be considered as an indirect
45
46 proof of the presence of metals onto the carbon surface, even though they are not
47
48 directly determined by XPS.
49
50
51
52
53
54

55
56 Electrochemical results are collectively reported in Fig. 5 to permit comparison of the
57
58 many materials obtained with variable relative Fe/Cu weight amounts and a constant,
59
60 equimolar Glu/Hist ratio. Results only concern T=900 °C given that weak or no activity

1
2
3
4
5
6 was observed for $T=600$ °C. All curves are net oxygen reduction currents, corrections
7
8 for background residual currents and surface area normalization having been applied as
9
10 described in the Experimental. Metal addition affects both incipient oxygen reduction
11
12 potentials and currents. Notably enough, currents at first sharply increase by addition of
13
14 Cu only (curve B) to the metal-free reference (curve A), and approach a limiting current
15
16 behaviour at most negative potentials. Substituting a fractional Fe amount (25%) for Cu
17
18 (curve C) causes the incipient oxygen reduction potential to shift anodic by ~ 0.2 V at
19
20 the expense however of a decrease in current that becomes comparable to those of the
21
22 Glu/Hist blank. Thereafter, any increase in fractional Fe amount is accompanied by
23
24 gradually increasing currents, better approaching a diffusion mass transport behaviour,
25
26 with some, though limited, further increase in incipient reduction potentials. Figs. 6a, 6b
27
28 are an overview outlining the observed metal dependence of oxygen reduction currents
29
30 and incipient reduction potentials (at $\omega=700$ rpm, constant) in comparison with similar
31
32 values recorded on a commercial Pt catalyst (EC-20). In Fig. 6a two series of incipient
33
34 potential data are used, a first set of values being rather qualitatively based on “kink”
35
36 potentials at the cross-over point between a first, generally flat, and a second rising part
37
38 of each I/E curve; the second set relying instead more quantitatively on the peak
39
40 potential of a characteristic current maximum recorded at $\omega=0$ rpm [52] (such results
41
42 are not reported for brevity). In Fig. 6a incipient potentials increase with increasing
43
44 fractional Fe amount and reach well defined, limiting high values for Fe/Cu greater than
45
46 ~ 50 wt %, lower than the corresponding Pt values by ~ 40 -50 mV. A similar increasing
47
48 trend occurs for currents (Fig. 6b), without however any plateau and a maximum value
49
50 at 100 wt % Fe.
51
52
53
54
55
56
57
58
59
60

1
2
3
4
5
6 Then, we are left with open conclusions. On the one side, ORR behaviour improves
7
8 with increasing Fe/Cu ratio, reaching however a maximum in the presence of Fe only,
9
10 in the absence of a second metal (Cu), thus making uncertain that both metals are
11
12 essential to catalytic ORR activity. Given the above XPS results, in both instances the
13
14 question arises if Fe metal, possibly buried in the carbon matrix and/or complexed with
15
16 nitrogen groups, is accessible, and to what extent, to the outside solution in order to
17
18 form catalytically effective centres. Problems also arise concerning electrode durability
19
20 given the limited amount of metal present as such or in ionic form.
21
22
23
24
25

26 Acknowledgements

27
28
29 Financial support from MIUR (Ministry of Instruction, University and Research) under
30
31 Firb 2001 (contract RBAU01844A), FISR 2001 under the NUME Project “Sviluppo di
32
33 membrane protoniche composite e di configurazioni elettrodiche innovative per celle a
34
35 combustibile con elettrolita polimerico”, and from Cariplo Foundation (Project
36
37 2008.2235) are gratefully acknowledged. Acknowledgments are due to Dr. Nadia Santo
38
39 (C.I.M.A., Centro Interdipartimentale di Microscopia Avanzata, Università degli Studi
40
41 di Milano) for careful TEM analyses.
42
43
44
45
46
47

48 References

- 49
50 [1] <http://platinumprice.org/platinum-price-history.html>
51
52 [2] http://www1.eere.energy.gov/hydrogenandfuelcells/mypp/pdfs/fuel_cells.pdf
53
54 [3] R. Jasinski, *Nature* **1964**, *201*, 1212.
55
56 [4] S. Gupta, D. Tryk, I. Bae, W. Aldred, E. Yeager, *J. Appl. Electrochem.* **1989**, *19*, 19.
57
58 [5] M. Lefèvre, E. Proietti, F. Jaouen, J.-P. Dodelet, *Science* **2009**, *324*, 71.
59
60

- 1
2
3
4
5
6 [6] M. Yuasa, A. Yamaguchi, H. Itsuki, K. Tanaka, M. Yamamoto, K. Oyaizu, *Chem.*
7
8 *Mater.* **2005**, *17*, 4278.
9
10 [7] N. P. Subramanian, S.P. Kumaraguru, H. Colon-Mercado, H. Kim, B. N. Popov, T.
11
12 Black, D. A. Chen, *J. Power Sources* **2006**, *157*, 56.
13
14 [8] E. B. Easton, A. Bonakdarpour, R. Yang, D. A. Stevens, J. R. Dahn, *J. Electrochem.*
15
16 *Soc.* **2008**, *155*, B547.
17
18 [9] J. Maruyama, I. Abe, *Chem. Commun.* **2007**, *2007*, 2879.
19
20 [10] T. E. Wood, Z. Tan, A. K. Schmoeckel, D. O'Neill, R. Atanasoski, *J. Power*
21
22 *Sources* **2008**, *178*, 510.
23
24 [11] A. Garsuch, K. MacIntyre, X. Michaud, D. A. Stevens, J. R. Dahn, *J. Electrochem.*
25
26 *Soc.* **2008**, *155*, B953.
27
28 [12] T. Schilling, M. Bron, *Electrochim. Acta* **2008**, *53*, 5379.
29
30 [13] A. H. C. Sirk, S. A. Campbell, V. I. Birss, *J. Electrochem. Soc.* **2008**, *155*, B592.
31
32 [14] J. Maruyama, N. Fukui, M. Kawaguchi, I. Abe, *J. Power Sources* **2008**, *182*, 489.
33
34 [15] V. Nallathambi, J.-W. Lee, S. P. Kumaraguru, G. Wu, B. N. Popov, *J. Power*
35
36 *Sources* **2008**, *183*, 34.
37
38 [16] O. Ikeda, H. Fukuda, H. Tamura, *J. Chem. Soc., Faraday Trans.* **1986**, *82*, 1561.
39
40 [17] R. Holze, I. Vogel, W. Vielstich, *J. Electroanal. Chem.*, **1986**, *210*, 277.
41
42 [18] S. Dong and R. Jiang, *Ber. Bunsenges. Phys. Chem.* **1987**, *91*, 479.
43
44 [19] T. Sawaguchi, T. Itabashi, T. Matsue, I. Uchida, *J. Electroanal. Chem.* **1990**, *279*,
45
46 219.
47
48 [20] A. Widelöv, R. Lasson, *Electrochim. Acta* **1992**, *37*, 187.
49
50 [21] A. Widelöv, *Electrochim. Acta* **1993**, *38*, 2493.
51
52
53
54
55
56
57
58
59
60

- 1
2
3
4
5
6 [22] B. Bittins-Cattaneo, S. Wasmus, B. Lopez-Mishima, V. Vielstiech, *J. Appl.*
7
8 *Electrochem.* **1993**, 23, 625.
9
- 10 [23] G. Faubert, G. Lalande, R. Côté, D. Guay, J.P. Dodelet, L.T. Weng, P. Bertrand, G.
11
12 Dénès, *Electrochim. Acta* **1996**, 41, 1689.
13
- 14 [24] G. Faubert, R. Côté, D. Guay, J.P. Dodelet, G. Dénès, P. Bertrand, *Electrochim.*
15
16 *Acta* **1998**, 43, 341.
17
- 18 [25] A.L. Bouwkamp-Wijnoltz, W. Visscher and J.A.R. van Veen, *Electrochim. Acta*
19
20
21 **1998**, 43, 3141.
22
- 23 [26] S.L. Gojković, S. Gupta, R.F. Savinell, *J. Electroanal. Chem.* **1999**, 462, 63.
24
- 25 [27] R. Jiang, D. Chu, *J. Electrochem. Soc.* **2000**, 147, 4605.
26
- 27 [28] M. Lefèvre, J.P. Dodelet, P. Bertrand, *J. Phys. Chem. B* **2000**, 104, 11238.
28
- 29 [29] M. Lefèvre, J.P. Dodelet, P. Bertrand, *J. Phys. Chem. B* **2002**, 106, 8705.
30
- 31 [30] A.L. Boukamp-Wijnoltz, W. Visscher, J.A.R. van Veen, E. Boellaard, A.M. van
32
33 der Kraan, S.C. Tang, *J. Phys. Chem. B* **2002**, 106, 12993.
34
- 35 [31] M. Lefèvre, J.P. Dodelet, *Electrochim. Acta* **2003**, 48, 2749.
36
- 37 [32] H. Schulenburg, S. Stankov, V. Schulnemann, J. Radnik, I. Dorbandt, S. Fiechter,
38
39 P. Bogdanoff, H. Tributsch, *J. Phys. Chem. B* **2003**, 107, 9034.
40
- 41 [33] J.A.R. van Veen, H.A. Colijn, J.F. van Baar, *Electrochim. Acta* **1988**, 33, 801.
42
- 43 [34] G. Lalande, G. Faubert, R. Côté, D. Guay, J.P. Dodelet, L.T. Weng, P. Bertrand, *J.*
44
45 *Power Sources* **1996**, 61, 227.
46
- 47 [35] M. Bron, J. Radnik, M. Fieber-Erdmann, P. Bogdanoff, S. Fiechter, *J. Electroanal.*
48
49 *Chem.* **2002**, 535, 113.
50
- 51 [36] K. Sawai, N. Suzuki, *J. Electrochem. Soc.* **2004**, 151, A2132.
52
- 53 [37] R. Bashyam, P. Zelenay, *Nature* **2006**, 443, 63.
54
55
56
57
58
59
60

- 1
2
3
4
5
6 [38] K. Lee, L. Zhang, H. Lui, R. Hui, Z. Shi, J. Zhang, *Electrochim. Acta* **2009**, *54*,
7
8 4704.
9
- 10 [39] Y. Ma, P. B. Balbuena, *Chem. Phys. Lett.* **2007**, *440*, 130.
11
- 12 [40] E. Antolini, *Appl. Catal. B* **2009**, *88*, 1.
13
- 14 [41] J. Herranz, M. Lefèvre, J.-P. Dodelet, *J. Electrochem. Soc.* **2009**, *156*, B593.
15
- 16 [42] C. W. B. Bezerra, L. Zhang, K. Lee, H. Liu, A. L. B. Marques, E. P. Marques, H.
17
18 Wang, J. Zhang, *Electrochim. Acta* **2008**, *53*, 4937.
19
- 20 [43] P. Wang, Z. Wang, L. Jia, Z. Xiao *Phys. Chem. Chem. Phys.* **2009**, *11*, 2730.
21
- 22 [44] R. Fu, N. Yoshizawa, M. S. Dresselhaus, G. Dresselhaus, J. H. Satcher Jr., T. F.
23
24 Baumann, *Langmuir* **2002**, *18*, 10100.
25
- 26 [45] D. Hulicova-Jurcakova, M. Seredych, G.Q. Lu, T. J. Bandosz *Adv. Funct. Mater.*
27
28 **2009**, *19*, 438.
29
- 30 [46] S. Biniak, G. Szymański, J. Siedlewski, A. Świątkowski, *Carbon* **1997**, *35*, 1799.
31
- 32 [47] D. Long, J. Zhang, J. Yang, Z. Hu, G. Cheng, X. Liu, R. Zhang, L. Zhan, W. Qiao,
33
34 L. Ling, *Carbon* **2008**, *46*, 1253.
35
- 36 [48] J. R. Pels, F. Kapteijn, J. A. Moulijn, Q. Zhu, K. M. Thomas, *Carbon* **1995**, *33*,
37
38 1641.
39
- 40 [49] R. A. Sidik, A. B. Anderson, N. P. Subramanian, S. P. Kamaraguru, B. N. Popov,
41
42 *J. Phys. Chem. B* **2006**, *110*, 1787.
43
- 44 [50] N. P. Subramanian, X. Li, V. Nallathambi, S. P. Kumaraguru, H. Colon-Mercado,
45
46 G. Wu, J.-W. Lee, B. N. Popov, *J. Power Sources* **2009**, *188*, 38.
47
- 48 [51] R. Kothandaraman, V. Nallathambi, K. Artyushkova, S. Calabrese Barton, *Appl.*
49
50 *Cat. B* **2009**, *92*, 209.
51
52
53
54
55
56
57
58
59
60

1
2
3
4
5
6 [52] F. Jaouen, S. Marcotte, J.-P. Dodelet, G. Lindbergh, *J. Phys. Chem. B* **2003**, *107*,
7
8 1376.
9
10
11
12
13
14
15
16
17
18
19
20
21
22
23
24
25
26
27
28
29
30
31
32
33
34
35
36
37
38
39
40
41
42
43
44
45
46
47
48
49
50
51
52
53
54
55
56
57
58
59
60

For Peer Review

Figure Captions

Figure 1. TEM image of Glu sample ($T=600^{\circ}\text{C}$).

Figure 2. Pore Size Distributions at different temperatures. GluHistFe75.

Figure 3. Pore Size Distributions at various Glu/Hist molar ratios ($T=600^{\circ}\text{C}$).

Figure 4. High resolution Nitrogen (N1s) Spectra of GluHist: a) $T=600^{\circ}\text{C}$; b) $T=900^{\circ}\text{C}$. 1) pyridinic N (N6) (B.E. 398-398.4 eV); 2) pyrrolic-N in five member ring and/or pyridonic-N (N5) (B.E. 400-400.5 eV); 3) quaternary-N (NQ), *e.g.* N in graphene structure (B.E. 401.5-402.2 eV); 4) pyridinic-N-oxide (NX) (B.E. 403.5-404.8 eV) B.E. are from [45-48].

Figure 5. Voltammograms in oxygen-saturated 0.1M HClO_4 . A) GluHist; B) GluHistFe0; C) GluHistFe25; D) GluHist75; E) GluHistFe100. ($T=25^{\circ}\text{C}$; scan rate 5 mV s^{-1} ; rotation rate 700 rpm).

Figure 6. a) Incipient oxygen reduction potentials at different Fe wt %: ● and --- (heavy dashes) potentials at the intersection points in Fig. 5; ○ and ... (light dashes) peak potentials of cathodic maxima at $\omega=0$ rpm. Dashes are for EC-20 Pt catalyst, open and closed points are for home made carbons.

b) Currents at $E=+0.420\text{ V NHE}$ at different wt % Fe.

Lines are a guide to the eye. Error bars represent standard deviation of experimental data. (0.1M HClO_4 ; scan rate 5 mV s^{-1} ; rotation rate 700 rpm; $T=25^{\circ}\text{C}$.)

Tables

Table 1. Specific Surface Area ($\text{m}^2 \text{g}^{-1}$)

	Glu/Hist Molar Ratio	Fe/Cu wt%	Surface Area ($\text{m}^2 \text{g}^{-1}$) (T= 600°C)	Surface Area ($\text{m}^2 \text{g}^{-1}$) (T= 900°C)	S₉₀₀/S₆₀₀
Glu no silica	1/0	-	25	-	-
Glu	1/0	-	1143	-	-
GluHist0.1	1/0.10	-	950	714	0.75
GluHist0.25	1/0.25	-	728	700	0.96
GluHist0.50	1/0.50	-	813	-	-
GluHist	1/1	-	603	541	0.90
GluHistFe0	1/1	0 / 100	670	564	0.84
GluHistFe25	1/1	25 / 75	-	555	-
GluHistFe50	1/1	50 / 50	696	559	0.80
GluHistFe75	1/1	75 / 25	665	589	0.88
GluHistFe100	1/1	100 / 0	698	587	0.84

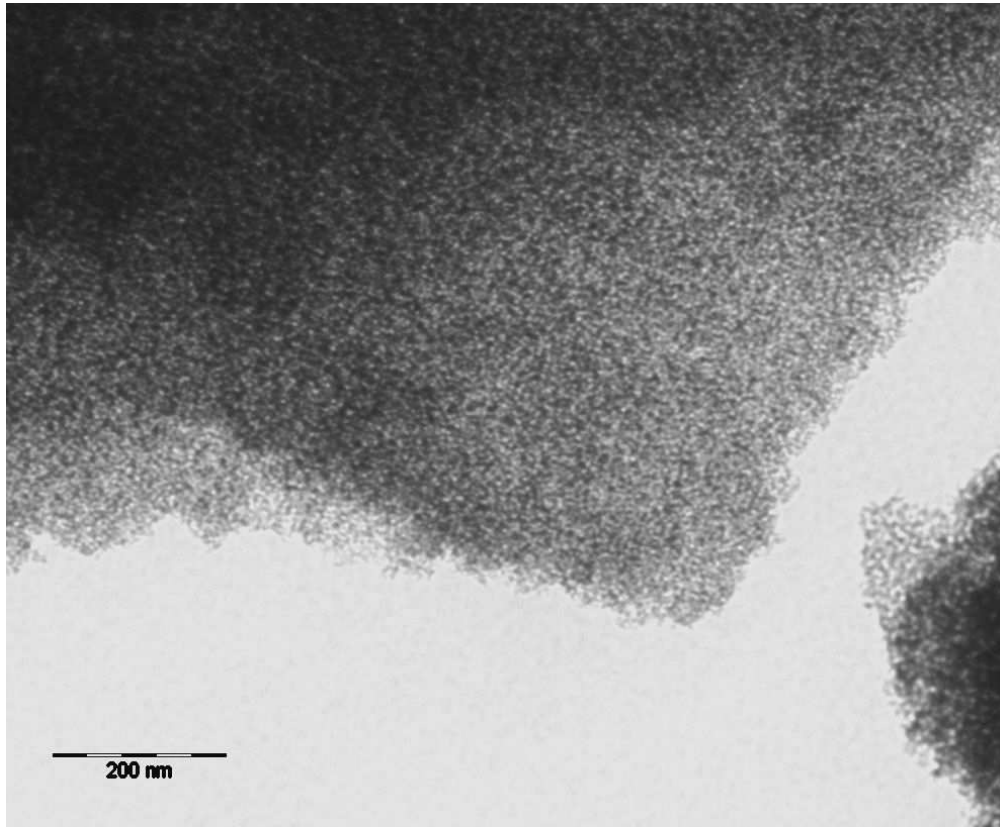
Table 2. Atomic C, O, N Percent Sample Compositions

	N 1s%		O 1s%		C 1s %	
	T= 600°C	T= 900°C	T= 600°C	T= 900°C	T= 600°C	T= 900°C
Glu	-	-	6	-	94	-
GluHist	14	7	4	2	82	91
GluHist0.10	4	4	5	2	91	94
GluHistFe0	14	-	4	-	82	-
GluHistFe50	13	7	5	2	82	91
GluHistFe75	13	8	5	2	83	90

Table 3. Atomic N Percent Sample Compositions

	B.E. eV	Description	GluHist		GluHistFe50		GluHistFe75	
			T= 600°C	T= 900°C	T= 600°C	T= 900°C	T= 600°C	T= 900°C
N6*	398.0-398.4	pyridinic N	36	27	39	37	38	36
N5*	400.0-400.5	pyrrolic-N in five member ring and or pyridonic-N	55	14	48	48	51	45
NQ*	401.5-402.2	quaternary-N	5	52	4	5	8	16
NX*	403.5-404.8	pyridinic-N-oxide	4	7	9	10	3	3

* Specification in the text



34
35
36
37
38
39
40
41
42
43
44
45
46
47
48
49
50
51
52
53
54
55
56
57
58
59
60

TEM image of Glu sample (T= 600°C).
349x288mm (72 x 72 DPI)